

Article

Effect of Ethanol on the Morphology and Textual Properties of ZSM-5 Zeolite

Xiuru Liu * and Yiqing Sun

Huadian electric power research Institute Co., LTD, Hangzhou 310030, China; yiqing-sun@chder.com

* Correspondence: xiuru-liu@chder.com; Tel.: +86-10-59216262

Received: 28 December 2019; Accepted: 4 February 2020; Published: 6 February 2020



Abstract: The morphology of ZSM-5 zeolite impacts the adsorption, separation and diffusion of molecules. The morphology and textual properties of ZSM-5 zeolites were adjusted by regulating the content of ethanol in the synthesis gel. When the ratio of ethanol/SiO₂ was lower than 2, the obtained crystals were isolated particles. With higher ethanol concentration, the chainlike zeolite was generated due to the condensation of terminal Si-OH groups. The crystals stacked more and more compactly with the increase in ethanol concentration, resulting in decreased specific surface area, total volume and mesoporous volume. The crystal size increased gradually with the increase in the ethanol concentration. Moreover, some other small molecular alcohols could also induce the formation of chainlike morphology of ZSM-5.

Keywords: ethanol; textual property; morphology; chainlike ZSM-5

1. Introduction

ZSM-5 zeolite shows a high thermal stability, anti-coke ability and excellent shape selectivity due to its acid property, exceptional skeleton and channel structure. It is widely used in petrochemical engineering [1–5], environmental pollution remediation [6,7] by adsorption and separation [8,9].

Among the physical properties of ZSM-5 zeolite, morphology is one of the dominated factors affecting its catalytic activity [10]. It impacts the diffusion, adsorption and separation of the reactant directly. The nano-sized zeolite showed a larger external surface area, a shorter diffusion length and a larger pore opening than the micro-sized zeolite [11]. Tago et al. [12,13] studied the influence of crystal size on the catalytic performance of ZSM-5 on *n*-hexane cracking. They found the reaction rate could be enhanced significantly by nanosizing zeolite. It exhibited a high catalytic stability on *n*-hexane cracking since it was less sensitive to the deactivation by coke [14]. The MFI zeolite with ultrathin nanosheet morphology showed a higher BET surface area and pore volume, which facilitated the transport of reactants, resulting in higher activity comparing with the conventional ZSM-5 zeolite [15–17]. The ZSM-5 zeolite with a hollow fiber morphology facilitated the cracking of *n*-butane and the generation of light alkenes due to the hierarchical porosity [18]. The self-stacked MFI zeolite prepared with the assistance of cationic polymers showed high activity in 1,3,5-triisopropylbenzene cracking and methanol-to-olefins reaction [19]. The chainlike ZSM-5 zeolite with a long pathway along *b*-axis prepared with sucrose as the second template enhanced the yield of 2, 6-dimethylnaphthalene [20]. Dong et al. [21] found that the diffusion of xylene isomers in the chainlike ZSM-5 zeolite is different due to its increased tortuosity of micropore in the crystal; thus, it has the potential for gas separation.

During the synthesis process of ZSM-5 zeolite, many factors, including temperature, duration of aging/hydrothermal treatment, composition of the synthesis gel and structure-directing agent, can influence its morphology. When the ratio of H₂O/SiO₂ increased, the crystal size of prepared ZSM-5 zeolite increased gradually [22]. When ethanol was used as the structure-directing agent, a coffin-shaped ZSM-5 zeolite was synthesized. However, a spherical shape ZSM-5 aggregated by primary nanocrystals

was synthesized by using tetrapropylammonium bromide as the structure-directing agent [23]. Lin et al. [24] prepared a ZSM-5 nanocrystal with the assistance of MFI precursor and polyacrylamide (PAM). At a relatively low temperature, monolithic nanocrystal agglomerated with a large number of intercrystal mesopore was synthesized, while at a higher temperature, cuplike ZSM-5 nanocrystals generated due to nucleation promotion and crystal growth restriction by MFI precursor and PAM. During the preparation of ZSM-5 zeolite, it takes some time to nucleate and grow. However, extending the reaction time further would cause the formation of silica [25]. By increasing the ratio of $\text{H}_2\text{O}/\text{SiO}_2$ from 40 to 80 or decreasing the ratio of NaOH/SiO_2 from 0.5 to 0.3 in the synthesis gel, the crystal sized increased gradually [26]. For chainlike ZSM-5 zeolite, another template or microwave treatment was necessary to induce the ordered stacking, which was costly and complicated. Chen et al. found that the alcohol with dielectric constant lower than 41.0 could facilitate the formation of Si-OH groups on the surface of zeolite crystals [27,28]. Then the Si-OH groups would undergo further condensation to form self-stacked morphology with the assistance of microwave irradiation. With the increase of microwave power, more and more stacking layers formed. It was explained that the high microwave power induced the condensation of hydroxyl groups and formed stacked crystals [29]. Chain-like silica nanocrystals were also prepared with the assistance of cationic polyelectrolyte [30]. Similarly, self-stacked MFI zeolite was prepared with cationic polymer as a second template [19]. The cationic polymer may reduce the interface surface tension, resulting in the stacking of crystals.

Therefore, it is meaningful and important to develop a facile synthetic strategy to control the morphology and crystal size of ZSM-5. In this study, a facile method to regulate the morphology of ZSM-5 zeolite from isolated nano-crystal to chainlike crystal was developed by adjusting the ethanol concentration in the synthesis gel. The crystal size from submicron to nanosize can also be effectively regulated. Moreover, the relationship between morphology and textual properties was studied in detail.

2. Results and Discussion

2.1. ZSM-5 Zeolite Synthesized after Evaporating Ethanol for Different Periods

The XRD patterns of ZSM-5 zeolite synthesized after evaporating ethanol for different time are shown in Figure 1. They show the same diffraction peaks and the intensity are comparative, indicating that this process had little influence on the crystal structure. The SEM images of ZSM-5 zeolite synthesized after evaporating ethanol for different time are shown in Figure 2. With the increase of evaporation time, the ethanol content in the liquid decreased. For the untreated sample, some crystals stacked together and formed the chainlike zeolite. With the decrease of ethanol, the chainlike zeolite decreased and the isolated crystals increased. Moreover, the crystal size also decreased gradually. Therefore, ethanol could play an important role in the formation of chainlike zeolite and a higher ethanol concentration could be beneficial for chainlike zeolite formation.

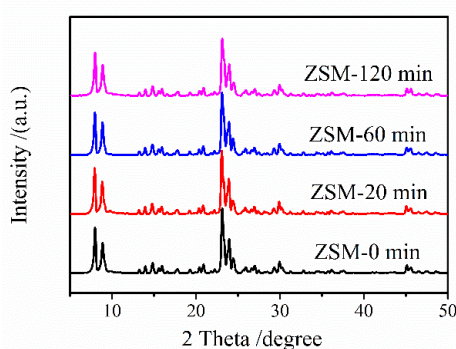


Figure 1. XRD patterns of ZSM-5 synthesized after evaporating ethanol for different times.

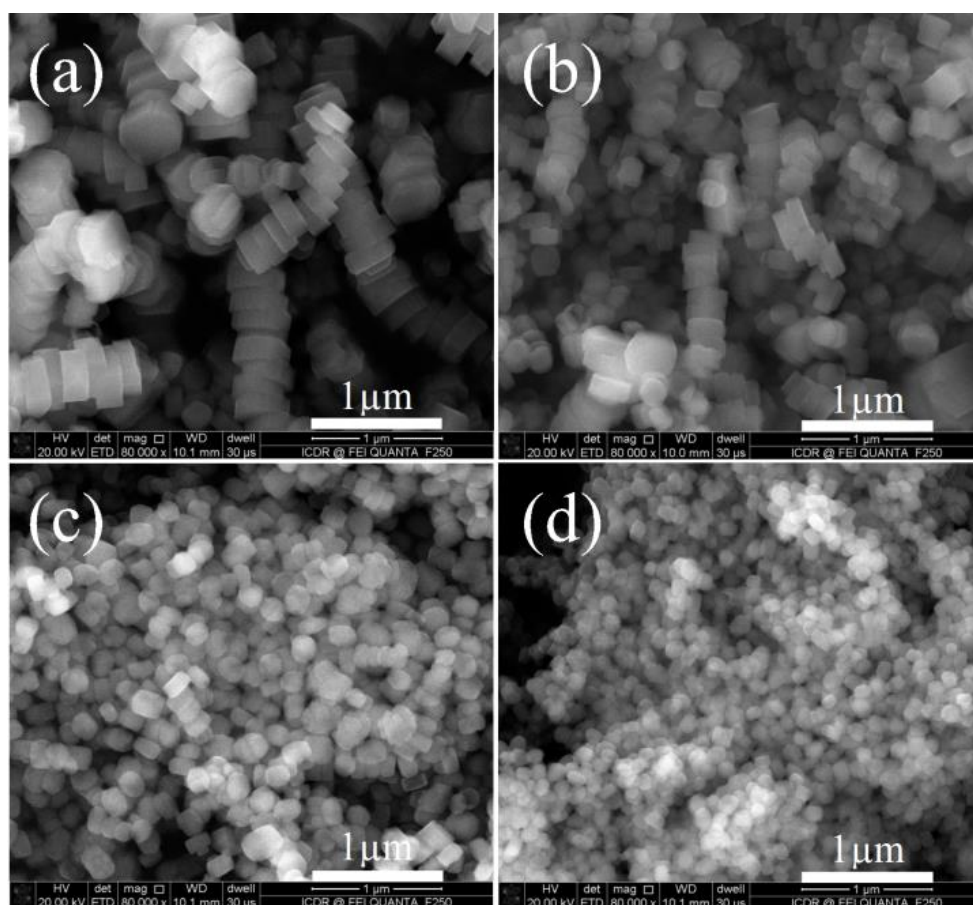


Figure 2. SEM images of ZSM-5 zeolite synthesized after evaporating ethanol for different time. (a) ZSM5—0 min; (b) ZSM5—20 min; (c) ZSM5—60 min; (d) ZSM5—120 min.

2.2. Effect of Ethanol Content on ZSM-5 Zeolite Morphology

The effect of ethanol content on the morphology of ZSM-5 was studied and the SEM pictures of the samples prepared with different ethanol concentrations are shown in Figure 3. At a relatively lower ratio (ethanol/SiO₂ ≤ 2), the synthesized crystals were individual and the crystal size increased gradually with the increase in the ethanol concentration (Figure 3a–c). When the ethanol concentration (2 < ethanol/SiO₂ < 5) increased further, the ratio of chainlike ZSM-5 zeolite increased (Figure 3d,e). When ethanol/SiO₂ ratio was higher than 5, most crystals stacked compactly (Figure 3f–h). The XRD patterns in Figure 4 all show the same characteristic diffraction peaks between 7°–9° and 23°–25°. Little impurity existed in the samples. The relative crystallinity was calculated according to the intensity of five peaks at 8.0°, 8.9°, 23.1°, 23.9° and 24.4° [15]. The results are shown in Table 1. The relative crystallinity increased with the increase of ethanol concentration. This may be explained by the fact that ethanol can act as a second structure-directing agent, which facilitated the growth of crystal and increased the crystallinity [31]. In addition, from the FTIR patterns in Figure 5, the peaks at 1225 cm⁻¹, 1105 cm⁻¹, 800 cm⁻¹, 450 cm⁻¹ and 450 cm⁻¹ corresponding to MFI phase skeletal characteristic peaks [32–34] appeared in all the samples, indicating the generation of MFI skeleton, which is consistent with the results of the XRD patterns.

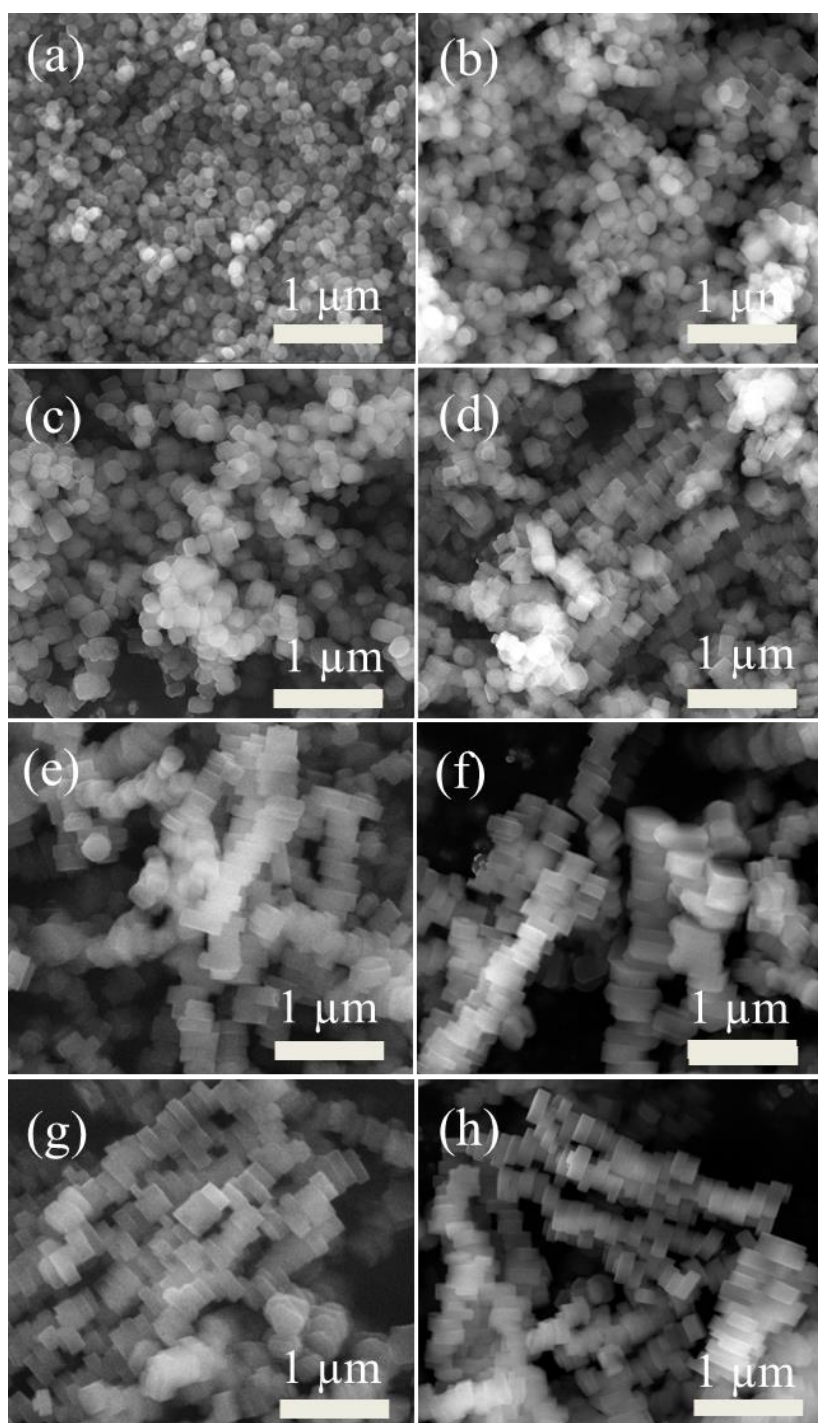


Figure 3. SEM images of ZSM5 zeolite prepared with different ethanol concentrations. (a) ZSM5-0; (b) ZSM5-1; (c) ZSM5-2; (d) ZSM5-4; (e) ZSM5-5; (f) ZSM5-6; (g) ZSM5-7; (h) ZSM5-8.

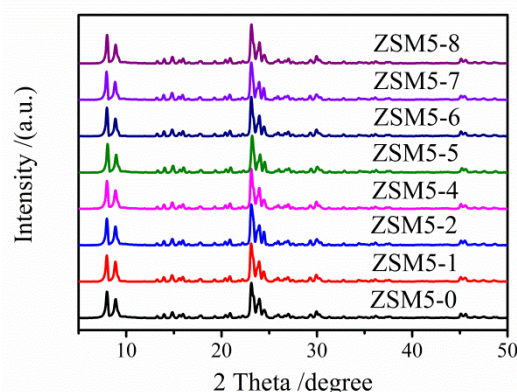


Figure 4. XRD patterns of ZSM-5 zeolite synthesized with different ethanol concentrations.

Table 1. Textual properties of ZSM-5 zeolites prepared with different ethanol concentrations.

Sample	R_c^a /%	S_{BET}^b / $m^2 \cdot g^{-1}$	V_{total}^c / $cm^3 \cdot g^{-1}$	V_{micro}^d / $cm^3 \cdot g^{-1}$	V_{meso}^e / $cm^3 \cdot g^{-1}$	P^f /nm
ZSM5-0	89.47	370.74	0.63	0.17	0.46	3.40
ZSM5-1	91.12	341.22	0.51	0.17	0.34	2.98
ZSM5-2	95.12	333.10	0.48	0.16	0.32	2.90
ZSM5-4	96.86	316.48	0.38	0.15	0.23	2.41
ZSM5-5	98.27	306.28	0.26	0.14	0.12	1.67
ZSM5-6	99.05	303.05	0.25	0.15	0.10	1.66
ZSM5-7	99.97	289.92	0.26	0.14	0.12	1.80
ZSM5-8	100.00	262.06	0.24	0.12	0.12	1.81

^a Relative crystallinity calculated from XRD pattern, the crystallinity of ZSM5-8 is considered as 100% [15]; ^b BET surface area; ^c Total volume adsorbed at $P/P_0 = 0.99$; ^d Micropore volume ($r < 2$ nm); ^e Mesopore volume, $V_{meso} = V_{total} - V_{micro}$; ^f Average pore radius.

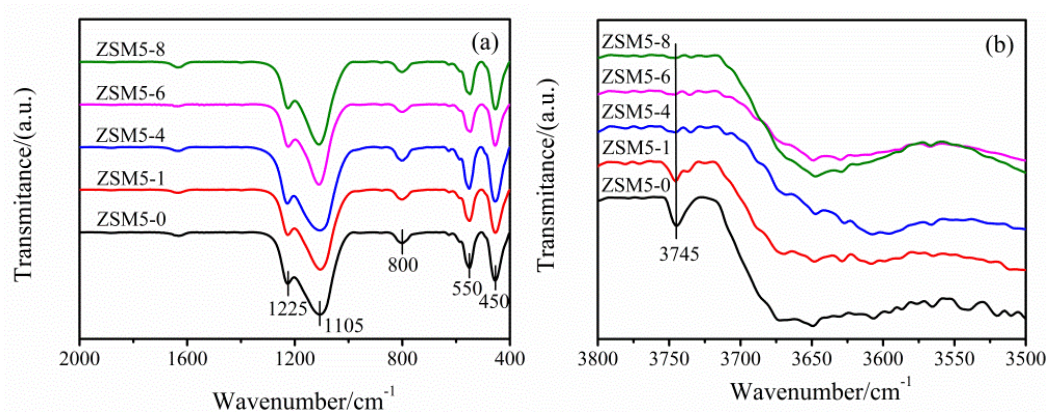


Figure 5. FTIR patterns of ZSM-5 zeolite synthesized with different ethanol concentrations, (a) 400–2000 cm^{-1} , (b) 3500–3800 cm^{-1} .

The N_2 adsorption-desorption isotherms and pore-size distribution curves of ZSM-5 zeolite synthesized with different ethanol concentration are shown in Figure 6. The scopes of isotherms increase gradually with the decrease in ethanol concentration. The hysteresis loops appear obviously when the ratio of ethanol/ SiO_2 is lower than 2. This indicates large mesopores or macropores, which is consistent with the results of the pore-size distribution curves. With the increase of individual crystals and the decrease of crystal size, the crystal stacked randomly and generated more and more intercrystal mesopore. The textual properties of ZSM-5 zeolites prepared with different ethanol concentrations in the gel are shown in Table 1. The specific surface area, total volume and mesopore volume decreased

with the increase of ethanol content. As the crystals stacked more and more compactly, less surface of the crystal was exposed, resulting in a decrease of the BET surface area. Moreover, the crystal size increased and stacked together, leading to the decrease of intercrystal pore volume. On one hand, when the BET surface area decreased, less pore opening and active sites were exposed, resulting in a decreased activity in reactions catalyzed by acid sites in the micropore; on the other hand, the stacking of crystals increased the diffusion length and tortuosity of pore channels, which had great influence on the diffusion of molecules. The diffusion rate of molecules with different dynamic diameters was significantly different. Thus, it may be beneficial for the separation of molecules.

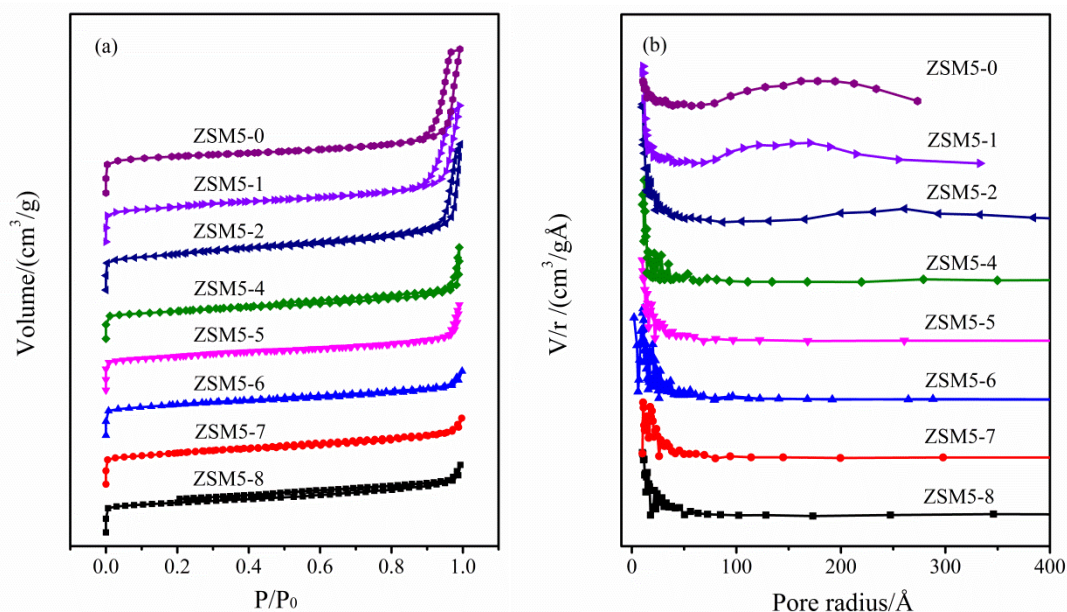


Figure 6. N_2 adsorption-desorption isotherms (a) and pore-size distributions (b) of ZSM-5 zeolite synthesized with different ethanol concentrations.

The NH_3 -TPD patterns of ZSM-5 zeolites synthesized with different ethanol concentrations are shown in Figure 7. Both strong acid peak and weak acid peak appeared in all the synthesized zeolites and they showed comparative acid amounts. The pyridine-absorbed FTIR spectra of ZSM-5 zeolites synthesized with different ethanol concentrations were determined and are shown in Figure 8. The peaks at 1450 cm^{-1} and 1550 cm^{-1} correspond to Lewis acid and Brønsted acid sites, respectively [3]. The amount of Brønsted acid was higher than that of Lewis acid, indicating that most aluminum atoms existed in the framework of zeolite. Moreover, the ratio of Brønsted/Lewis increased with the increase of ethanol concentration. On one hand, ethanol enhanced the nucleation and growth of crystal, which facilitated the cooperation of aluminum atoms into the framework, resulting in a higher Brønsted acid level; on the other hand, the BET surface area increased with the decrease of ethanol content. Thus, more acid sites were exposed on the external surface that were Lewis acid sites [35].

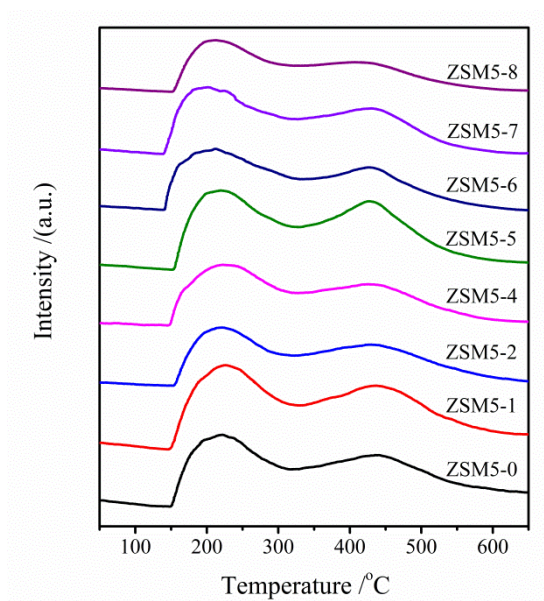


Figure 7. NH₃-TPD patterns of ZSM-5 zeolites synthesized with different ethanol concentrations.

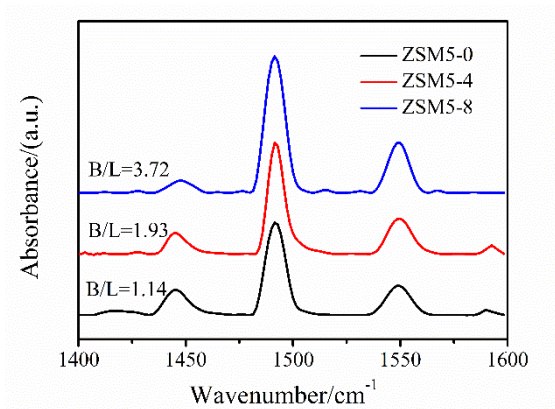


Figure 8. Pyridine-absorbed FTIR spectra of ZSM-5 synthesized with different ethanol concentrations.

2.3. Effect of Other Factors on the Morphology of ZSM-5

2.3.1. Effect of Alcohol Molecules

SEM images of ZSM-5 zeolite prepared with methanol, ethanol, ethylene glycol and isopropanol in the synthesis gel are shown in Figure 9. They showed a similar morphology. Some crystals stacked and generated chainlike zeolite. The other crystals existed individually. Therefore, the concentration of alcohol molecules in the synthesis gel, rather than the sort, could modify the nuclei and crystal surface, forming abundant hydroxyls, which is conducive to the stacking of zeolite crystals.

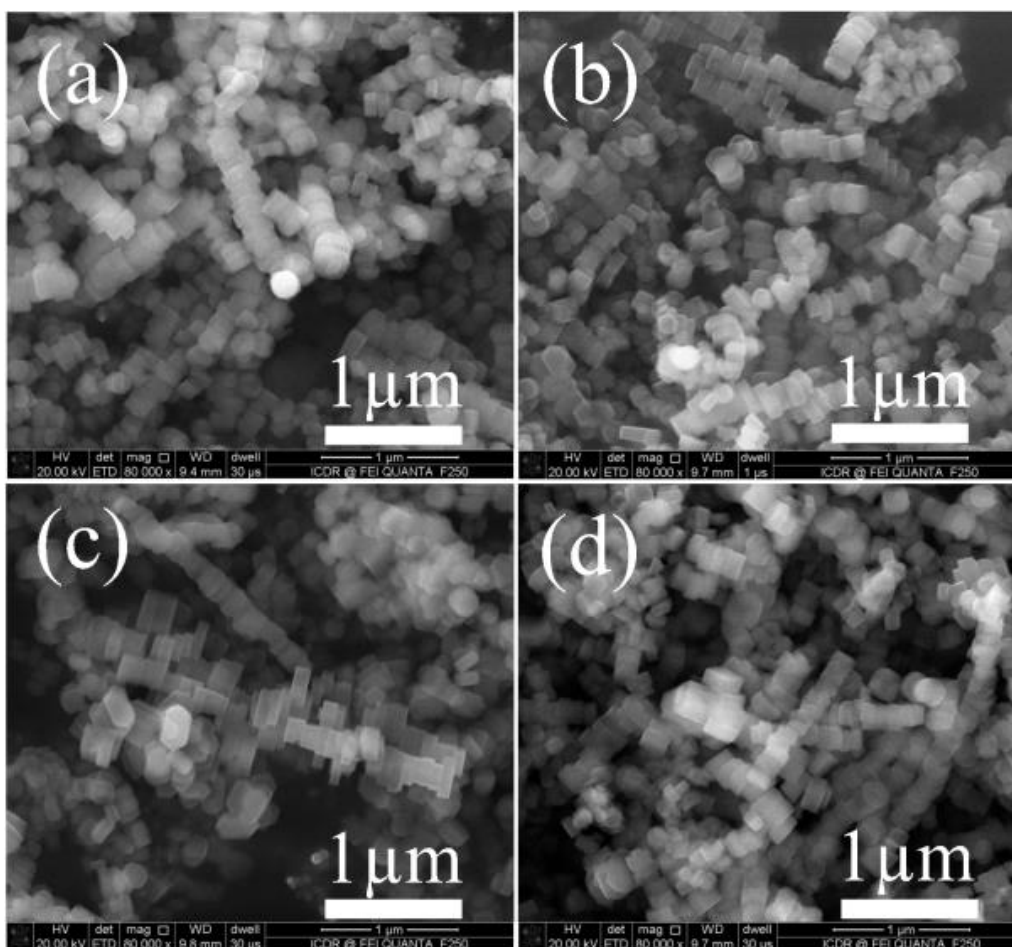


Figure 9. SEM images of ZSM-5 zeolite prepared with different alcohols in the synthesis gel. (a) methanol; (b) ethanol; (c) ethylene glycol; (d) isopropanol.

2.3.2. Effect of Heating on Morphology during Ethanol Evaporation

During ethanol evaporation in the preparation process, the solution was heated for a certain time. Thus, the influence of heating on the morphology of ZSM-5 was investigated by heating at 80 °C for 3 h hermetically. The SEM image of the synthesized ZSM-5 was shown in Figure 10. It exhibited both chainlike and individual morphology. This result suggests that heating at 80 °C could not guarantee the formation of chainlike zeolite and the morphology of chainlike zeolite shown in this figure is quite similar to that shown in Figure 2a. Therefore, it can be concluded that heating for ethanol evaporation could not decompose the chainlike zeolite and the isolated zeolite particles by evaporating ethanol could be due to the decrease in ethanol concentration, but not due to the heating at 80 °C.

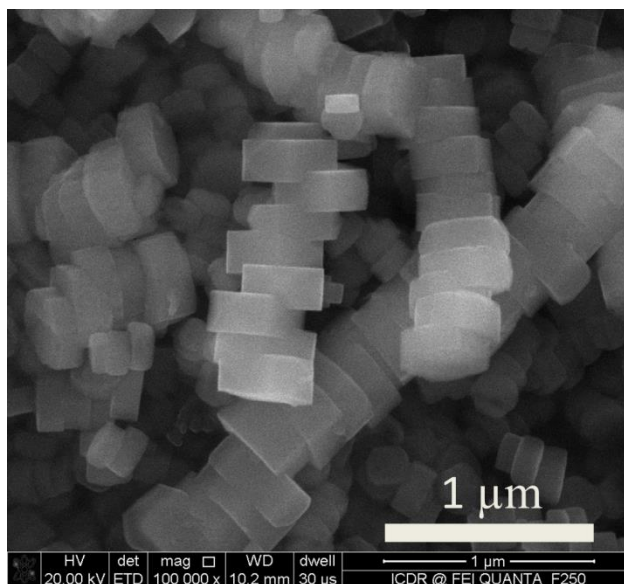


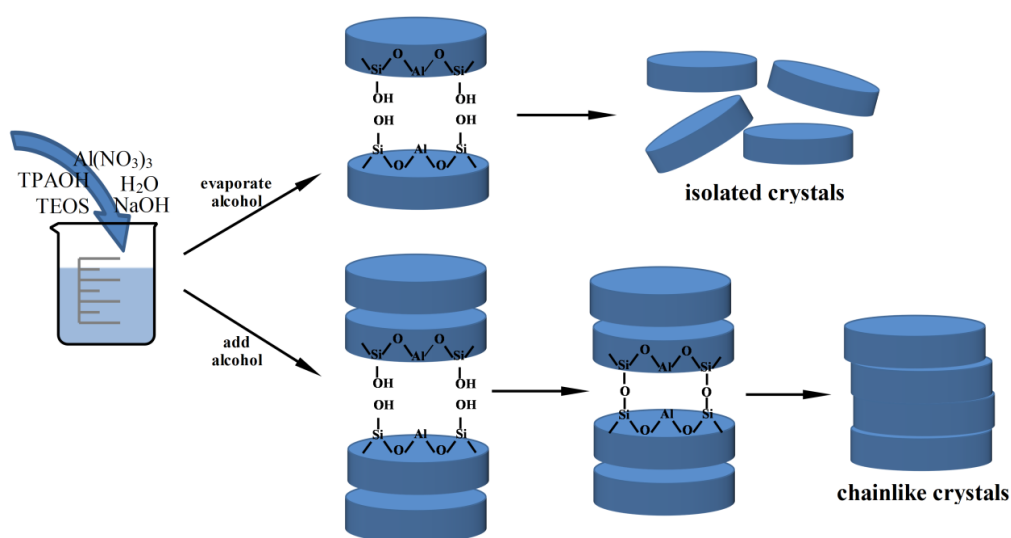
Figure 10. SEM image of ZSM-5 zeolite prepared with heating hermetically at 80 °C for 3 h.

2.4. Possible Mechanism for the Influence of Alcohol on the Morphology of Zeolite

According to the results and references, a possible mechanism for the influence of alcohol on the morphology of ZSM-5 zeolite was proposed. On the one hand, the ethanol molecules in the solution are easy to congregate with each other and form stable dimers [36–38]. The continuous chains of ethanol dimers occupied in the channels of ZSM-5 crystals and acted as structure-directing agent, which could also facilitate the stacking of crystals. It was reported that the C-OH groups in the sucrose could interact with aluminosilicate species through hydrogen bonding and induce the formation of chainlike structure [20]. Thus, the C-OH group in ethanol could play the same role and induce the formation of a chainlike structure. Chen et al. [28] found the alcohol with dielectric constant lower than 41.0 could facilitate the formation of the stacking structure.

On the other hand, the OH-region IR spectra of ZSM-5 zeolites synthesized with different ethanol concentrations are shown in Figure 5b. With the increase of ethanol, the peaks at 3745 cm^{-1} (terminal Si-OH) decreased gradually. It was reported that the condensation of dissociative Si-OH groups on the (010) surface was energetically favorable [39]. Large Si-OH groups on the crystal surface were unstable [21]. Thus, ethanol could promote the stacking of zeolite crystals. Moreover, it was believed that ethanol in the synthesis gel could facilitate the nucleation and growth of crystals [31,40]. Thus the crystal size decreased when the ethanol concentration decreased.

The illustration for the influence of alcohol on the morphology is shown in Scheme 1. With a relatively high alcohol concentration, terminal Si-OH groups between the adjacent crystals condensed and generated ordered stacking, while for a relatively low alcohol content, terminal Si-OH groups would not react with each other, resulting in isolated crystals.



Scheme 1. Possible mechanism for the influence of alcohol on the morphology of ZSM-5 zeolite.

3. Experimental

3.1. Materials

Tetraethyl orthosilicate (TEOS), tetrapropylammonium hydroxide (TPAOH, 25 wt%), sodium hydroxide (NaOH), aluminium nitrate ($\text{Al}(\text{NO}_3)_3$), ethanol, ammonium nitrate (NH_4NO_3) and pyridine were purchased from Sinopharm Chemical Reagent Co. Ltd. (Shanghai, China) and used as received.

3.2. Synthesis of ZSM-5 Zeolite

The molar ratio of the components in synthesis gel was $100 \text{ SiO}_2 : 2 \text{ Al}_2\text{O}_3 : 24.6 \text{ TPAOH} : 5 \text{ Na}_2\text{O} : 1417 \text{ H}_2\text{O} : 400 \text{ ethanol}$. The schematic diagram of ZSM-5 zeolite synthesis is shown in Figure 11. Firstly, tetraethyl orthosilicate (25 g) was added into the solution of tetrapropylammonium hydroxide (24 g TPAOH, 25 wt%) and stirred for 4 h to obtain a clear solution. The solution was heated at 80°C for different times to evaporate ethanol. Then, the mixture of NaOH (0.24 g), $\text{Al}(\text{NO}_3)_3$ and H_2O (6.3 g) was added into the solution. The prepared solution was pre-aged at 25°C for 24 h. Finally, the pre-aged solution was transferred into a Teflon-lined stainless-steel autoclave and crystallized at 170°C for 24 h. The products were separated, washed and dried thoroughly. The Na-ZSM-5 can be obtained after removing the organic template by calcining at 550°C for 6 h. Then, it was ion-exchanged with NH_4NO_3 3 times, dried overnight and calcined at 550°C for 3 h to obtain H-ZSM-5. For convenience, the samples with evaporating ethanol were denoted as ZSM5-t min, where t represents the time for evaporating ethanol.

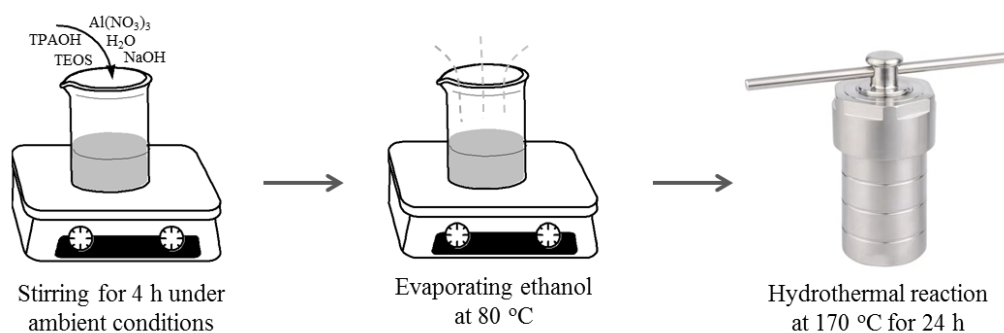


Figure 11. Schematic diagram of ZSM-5 zeolite synthesis.

In order to study the effect of ethanol concentration on the morphology, ethanol was evaporated absolutely firstly and then a certain amount of ethanol was added into the synthesis gel. The samples were denoted as ZSM5-X, where X represented the molar ratio of ethanol/SiO₂ in the synthesis gel. In addition, ethanol was evaporated absolutely firstly and followed by adding an equal amount of other alcohols (100 SiO₂: 2 Al₂O₃: 24.6 TPAOH: 5 Na₂O: 1417 H₂O: 400 alcohols, alcohols included methanol, ethanol, ethylene glycol and isopropanol) into the synthesis gel to study the influence of different alcohols.

In order to exclude the influence of heating during evaporation ethanol on the morphology of ZSM-5 zeolite, the synthesis gel was heated at 80 °C for 3 h hermetically, which prevented the evaporation of ethanol. The following process including pre-aging and a hydro-thermal synthesis process was conducted in the same way as the others.

3.3. Characterization

After calcination at 550 °C, the physicochemical properties of catalysts were determined. The XRD patterns were obtained on an X'pert PRO MRD diffractometer. The SEM images were conducted on FEI Quanta FEG 250. TEM images were recorded on JEOL JEM-2100. The textural properties were determined on Builder SSA-4200 instrument according to the N₂ adsorption-desorption measurement. The NH₃-TPD was obtained on Builder PCA-1200 according to [15]. A Bruker FT-IR spectrometer (SENSOR37) was used to record the FTIR and pyridine-absorbed FTIR spectra. Pyridine-absorbed FTIR was determined after absorbing pyridine at ambient temperature and desorbing pyridine at 150 °C.

4. Conclusions

In this work, ZSM-5 with individual or chainlike morphology was prepared by adjusting the ethanol concentration. When the ratio of ethanol/SiO₂ was lower than 2, the synthesized zeolite was isolated particles. With a higher ethanol concentration, the crystals stacked due to the condensation of Si-OH groups. The crystals stacked more and more compactly with the increase in the ethanol concentration, resulting in a decrease of the BET surface area and total volume. The crystal size increased gradually due to the facilitation of ethanol. Moreover, other small molecular alcohols, including methanol, ethylene glycol and isopropanol, could also induce the formation of a chainlike morphology. The ordered stacking of crystals would increase the tortuosity of the pore channels. The isolated nano-crystals showed a shorter diffusion length. They may show specific properties in adsorption and catalysis.

Author Contributions: X.L. did most of the experiments and wrote the manuscript; Y.S. did some of the experiments. All authors have read and agreed to the published version of the manuscript.

Funding: This work was financially supported by the funding named as 'Research and Application of Key Technologies for Blockage Control of Air Preheater in Coal-fired Power Plant (No. CHDKJ19-01-57).

Conflicts of Interest: The authors declare no conflict of interest.

References

1. Blay, V.; Louis, B.; Miravalles, R.; Yokoi, T.; Peccatiello, K.A.; Clough, M.; Yilmaz, B. Engineering Zeolites for Catalytic Cracking to Light Olefins. *ACS Catal.* **2017**, *7*, 6542–6566. [[CrossRef](#)]
2. Ji, Y.; Yang, H.; Zhang, Q.; Yan, W. Phosphorus modification increases catalytic activity and stability of ZSM-5 zeolite on supercritical catalytic cracking of n-dodecane. *J. Solid State Chem.* **2017**, *251*, 7–13. [[CrossRef](#)]
3. Ji, Y.; Yang, H.; Yan, W. Catalytic cracking of n-hexane to light alkene over ZSM-5 zeolite: Influence of hierarchical porosity and acid property. *Mol. Catal.* **2018**, *448*, 91–99. [[CrossRef](#)]
4. Ji, Y.; Yang, H.; Yan, W. Effect of alkali metal cations modification on the acid/basic properties and catalytic activity of ZSM-5 in cracking of supercritical n-dodecane. *Fuel* **2019**, *243*, 155–161. [[CrossRef](#)]

5. Standl, S.; Hinrichsen, O. Kinetic modeling of catalytic olefin cracking and methanol-to-olefins (MTO) over zeolites: A review. *Catalysts* **2018**, *8*, 626. [[CrossRef](#)]
6. Yuan, E.; Wu, G.; Dai, W.; Guan, N.; Li, L. One-pot construction of Fe/ZSM-5 zeolites for the selective catalytic reduction of nitrogen oxides by ammonia. *Catal. Sci. Technol.* **2017**, *7*, 3036–3044. [[CrossRef](#)]
7. Li, D.; Yao, J.; Sun, H.; Liu, B.; van Agtmaal, S.; Feng, C. Recycling of phenol from aqueous solutions by pervaporation with ZSM-5/PDMS/PVDF hollow fiber composite membrane. *Appl. Surf. Sci.* **2018**, *427*, 288–297. [[CrossRef](#)]
8. Zhang, Y.; Jin, F.; Shen, Z.; Lynch, R.; Al-Tabbaa, A. Kinetic and equilibrium modelling of MTBE (methyl tert-butyl ether) adsorption on ZSM-5 zeolite: Batch and column studies. *J. Hazard. Mater.* **2018**, *347*, 461–469. [[CrossRef](#)]
9. Briao, G.V.; Jahn, S.L.; Foletto, E.L.; Dotto, G.L. Adsorption of crystal violet dye onto a mesoporous ZSM-5 zeolite synthesized using chitin as template. *J. Colloid Interface Sci.* **2017**, *508*, 313–322. [[CrossRef](#)]
10. Ji, Y.; Yang, H.; Yan, W. Strategies to enhance the catalytic performance of ZSM-5 zeolite in hydrocarbon cracking: A review. *Catalysts* **2017**, *7*, 367. [[CrossRef](#)]
11. Mintova, S.; Gilson, J.P.; Valtchev, V. Advances in nanosized zeolites. *Nanoscale* **2013**, *5*, 6693–6703. [[CrossRef](#)] [[PubMed](#)]
12. Konno, H.; Tago, T.; Nakasaka, Y.; Ohnaka, R.; Nishimura, J.I.; Masuda, T. Effectiveness of nano-scale ZSM-5 zeolite and its deactivation mechanism on catalytic cracking of representative hydrocarbons of naphtha. *Micropor. Mesopor. Mat.* **2013**, *175*, 25–33. [[CrossRef](#)]
13. Nakasaka, Y.; Okamura, T.; Konno, H.; Tago, T.; Masuda, T. Crystal size of MFI-type zeolites for catalytic cracking of n-hexane under reaction-control conditions. *Micropor. Mesopor. Mat.* **2013**, *182*, 244–249. [[CrossRef](#)]
14. Mochizuki, H.; Yokoi, T.; Imai, H.; Watanabe, R.; Namba, S.; Kondo, J.N.; Tatsumi, T. Facile control of crystallite size of ZSM-5 catalyst for cracking of hexane. *Micropor. Mesopor. Mat.* **2011**, *145*, 165–171. [[CrossRef](#)]
15. Ji, Y.; Shi, B.; Yang, H.; Yan, W. Synthesis of isomorphous MFI nanosheet zeolites for supercritical catalytic cracking of n-dodecane. *Appl. Catal. A* **2017**, *533*, 90–98. [[CrossRef](#)]
16. Tian, Y.; Zhang, B.; Liang, H.; Hou, X.; Wang, L.; Zhang, X.; Liu, G. Synthesis and performance of pillared HZSM-5 nanosheet zeolites for n-decane catalytic cracking to produce light olefins. *Appl. Catal. A* **2019**, *572*, 24–33. [[CrossRef](#)]
17. Tian, Y.; Liu, H.; Wang, L.; Zhang, X.; Liu, G. Controllable fabrication and catalytic performance of nanosheet HZSM-5 films by vertical secondary growth. *AIChE J.* **2018**, *64*, 1923–1927. [[CrossRef](#)]
18. Han, J.; Jiang, G.; Han, S.; Liu, J.; Zhang, Y.; Liu, Y.; Wang, R.; Zhao, Z.; Xu, C.; Wang, Y.; et al. The fabrication of Ga₂O₃/ZSM-5 hollow fibers for efficient catalytic conversion of n-butane into light olefins and aromatics. *Catalysts* **2016**, *6*, 13. [[CrossRef](#)]
19. Wang, R.; Liu, W.; Ding, S.; Zhang, Z.; Li, J.; Qiu, S. Mesoporous MFI zeolites with self-stacked morphology templated by cationic polymer. *Chem. Commun.* **2010**, *46*, 7418–7420. [[CrossRef](#)]
20. Jin, L.; Xie, T.; Liu, S.; Li, Y.; Hu, H. Controllable synthesis of chainlike hierarchical ZSM-5 templated by sucrose and its catalytic performance. *Catal. Commun.* **2016**, *75*, 32–36. [[CrossRef](#)]
21. Sadighi, S.; Masoudian Targhi, S.K. Preparation of Biofuel from Palm Oil Catalyzed by Ammonium Molybdate in Homogeneous Phase. *Bull. Chem. React. Eng. Catal.* **2017**, *12*, 49. [[CrossRef](#)]
22. Sashkina, K.A.; Qi, Z.; Wu, W.; Ayupov, A.B.; Lysikov, A.I.; Parkhomchuk, E.V. The effect of H₂O/SiO₂ ratio in precursor solution on the crystal size and morphology of zeolite ZSM-5. *Micropor. Mesopor. Mat.* **2017**, *244*, 93–100. [[CrossRef](#)]
23. Ma, T.; Zhang, L.; Song, Y.; Shang, Y.; Zhai, Y.; Gong, Y. A comparative synthesis of ZSM-5 with ethanol or TPABr template: Distinction of Brønsted/Lewis acidity ratio and its impact on n-hexane cracking. *Catal. Sci. Technol.* **2018**, *8*, 1923–1935. [[CrossRef](#)]
24. Liu, R.; Lin, S.; Shi, L.; Gao, H.; Lv, M.; Tan, K.; Wang, R. Morphology adjustment of ZSM-5 nanocrystal agglomerates and achievement of improved activity in LDPE catalytic cracking reaction. *Micropor. Mesopor. Mat.* **2019**, *285*, 120–128. [[CrossRef](#)]
25. Sadeghpour, P.; Haghighi, M.; Shekari, P. Facile moderate-temperature hydrothermal design of nanocrystalline coffin-shaped ZSM-5 catalyst for transformation of CH₃OH to C₂H₄/C₃H₆. *Particul. Sci. Technol.* **2019**, *37*, 1–14. [[CrossRef](#)]

26. Zhao, Y.; Ye, Z.; Zhang, H.; Zhang, Y.; Tang, Y. Facile fabrication and morphology regulation of crossed mfi zeolite with improved performance on LDPE cracking. *Ind. Eng. Chem. Res.* **2019**, *58*, 13174–13181. [[CrossRef](#)]
27. Chen, X.; Yan, W.; Shen, W.; Yu, J.; Cao, X.; Xu, R. Morphology control of self-stacked silicalite-1 crystals using microwave-assisted solvothermal synthesis. *Micropor. Mesopor. Mat.* **2007**, *104*, 296–304. [[CrossRef](#)]
28. Chen, X.; Yan, W.; Cao, X.; Xu, R. Quantitative correlation between morphology of silicalite-1 crystals and dielectric constants of solvents. *Micropor. Mesopor. Mat.* **2010**, *131*, 45–50. [[CrossRef](#)]
29. Jin, H.; Jiang, N.; Park, S.E. Nanoarchitected synthesis of TS-1 depending on microwave power. *J. Phys. Chem. Solids* **2008**, *69*, 1136–1138. [[CrossRef](#)]
30. Aoki, K.; Mann, S. Polyelectrolyte-mediated synthesis and self-assembly of silicalite nanocrystals into linear chain superstructures. *J. Mater. Chem.* **2005**, *15*, 111. [[CrossRef](#)]
31. Zhang, Q.; Yang, H.; Yan, W. Effect of ethanol on the crystallinity and acid sites of MFI zeolite nanosheets. *RSC Adv.* **2014**, *4*, 56938–56944. [[CrossRef](#)]
32. Cheng, Y.; Wang, L.J.; Li, J.S.; Yang, Y.C.; Sun, X.Y. Preparation and characterization of nanosized ZSM-5 zeolites in the absence of organic template. *Mater. Lett.* **2005**, *59*, 3427–3430. [[CrossRef](#)]
33. Mohamed, R.M.; Fouad, O.A.; Ismail, A.A.; Ibrahim, I.A. Influence of crystallization times on the synthesis of nanosized ZSM-5. *Mater. Lett.* **2005**, *59*, 3441–3444. [[CrossRef](#)]
34. Mostafa, M.M.M.; Rao, K.N.; Harun, H.S.; Basahel, S.N.; El-Maksod, I.H.A. Synthesis and characterization of partially crystalline nanosized ZSM-5 zeolites. *Ceram. Int.* **2013**, *39*, 683–689. [[CrossRef](#)]
35. Lanzafame, P.; Barbera, K.; Perathoner, S.; Centi, G.; Aloise, A.; Migliori, M.; Macario, A.; Nagy, J.B.; Giordano, G. The role of acid sites induced by defects in the etherification of HMF on Silicalite-1 catalysts. *J. Catal.* **2015**, *330*, 558–568. [[CrossRef](#)]
36. Chiang, H.; Bhan, A. Catalytic consequences of hydroxyl group location on the rate and mechanism of parallel dehydration reactions of ethanol over acidic zeolites. *J. Catal.* **2010**, *271*, 251–261. [[CrossRef](#)]
37. Wang, C.H.; Bai, P.; Siepmann, J.I.; Clark, A.E. Deconstructing Hydrogen-Bond Networks in Confined Nanoporous Materials: Implications for Alcohol–Water Separation. *J. Phys. Chem. C* **2014**, *118*, 19723–19732. [[CrossRef](#)]
38. Arletti, R.; Fois, E.; Gigli, L.; Vezzalini, G.; Quartieri, S.; Tabacchi, G. Irreversible Conversion of a Water-Ethanol Solution into an Organized Two-Dimensional Network of Alternating Supramolecular Units in a Hydrophobic Zeolite under Pressure. *Angew. Chem. Int. Edit.* **2017**, *56*, 2105–2109. [[CrossRef](#)]
39. Quan, Y.; Li, S.; Wang, S.; Li, Z.; Dong, M.; Qin, Z.; Chen, G.; Wei, Z.; Fan, W.; Wang, J. Synthesis of Chainlike ZSM-5 Zeolites: Determination of Synthesis Parameters, Mechanism of Chainlike Morphology Formation, and Their Performance in Selective Adsorption of Xylene Isomers. *ACS Appl. Mater. Inter.* **2017**, *9*, 14899–14910. [[CrossRef](#)]
40. Uguina, M.A.; Lucas, A.D.; Ruiz, F.; Serrano, D.P. Synthesis of ZSM-5 from Ethanol-Containing Systems. Influence of the Gel Composition. *Ind. Eng. Chem. Res.* **1995**, *24*, 451–456. [[CrossRef](#)]

